33RD CONGRESS
OF THE INTERNATIONAL COUNCIL
OF THE AERONAUTICAL SCIENCES
STOCKHOLM, SWEDEN, 4–9 SEPTEMBER, 2022

ICAS 2022 SWEDEN

# DESIGN AND EFFICIENCY ANALYSIS OF EVTOL CONTRA-ROTATING PROPELER

Nanxuan Qiao[1,2], Tielin Ma[3,4], Xiangsheng Wang[1], JingchengFu[5]

[1] School of Aeronautic Science and Engineering, Beihang University, Beijing, PR China
[2] Shenyuan Honors College, Beihang University, Beijing 100191, PR China
[3] Institute of Unmanned System, Beihang University, Beijing, China
[4] Key Laboratory of Advanced Technology of Intelligent Unmanned Flight System, Ministry of Industry and Information Technology, Beijing, PR China
[5] School of Transportation Science and Engineering, Beihang University, Beijing 100191, PR China

## Abstract

With the continuous progress in the electric vertical take-off and landing (eVTOL) industry, the application of propellers on eVTOL aircrafts are becoming progressively mature. Contra-rotating propellers (CRPs) have the potential to generate significantly greater thrust with less power consumption than single propeller. In this paper, the ideal thrust and power consumption of the single propeller and dual propellers is calculated using the momentum theory and CFD actuator disc method. A CRP design optimization method is proposed with the actuator disc method and the Blade-element momentum method (BEM). The axial velocity extracted from the CFD actuator disc results is used to design and optimize the lower propeller. The design optimization method is verified by validation cases on an eVTOL CRP using the three-dimensional steady Reynolds-averaged Navier-Stokes solver and moving reference frames technique. The CFD results show that the optimized CRP hovering time is 12.7% higher than single propeller.

**Keywords:** eVTOL aircraft; Contra-rotating propeller; Blade shape; Optimization

## 1. General Introduction

Although the eVTOL industry has not developed for a long time, many companies have achieved remarkable results and solved the problems of capital, aviation cooperation and infrastructure. There are more than 150 relevant manufacturers and start-ups around the world committing to developing environmentally friendly suspends air taxis and ambulances, regional airliners and even unmanned delivery aircraft. However, before eVTOL aircrafts are widely used in urban air transportation, many technical difficulties need to be solved in aerodynamics[1], propulsion[2], control[3], vehicle safety[4], noise[5], [6], batteries[7] and multidisciplinary coupling optimization[8].

At present, studies have shown that compared with single propeller systems, CRP systems have the advantages of generating greater thrust, improving efficiency[9], reducing energy consumption[8], improving operation stability[6] and reducing the UAV's plan size. Toru Shigemitsu et al. used experiment and the numerical analysis to investigate the performance and the internal flow conditions between front and rear rotors of the contra-rotating small-sized axial fan[10]. Hoyun Jung et al. used numerical optimization to enhance the performance of the CRP and the best power coefficient value by optimized results is increased about 5% compare to the baseline model[11]. J.Tang et al. established an optimization approach to optimize and analyze the propulsion efficiency of the high-altitude contra-rotating propellers used Vortex Lattice Lifting Line Method with large blade aspect ratios[12].

The design optimization of CRPs needs to consider the interference between the two propellers, mainly the axial velocity between the two propellers. An acceptable result can be obtained by BEM method[13] or Vortex Lattice Lifting Line Method[12] with large blade aspect ratios. However, the empirical constants may differ for a different rotor blade planform and thrust which probably bring

uncertainty to the initial design process.

In this paper, a CRP design optimization method with high robustness and efficiency during initial design process is proposed with the CFD actuator disc method and BEM method. The design optimization method is verified by validation cases on the eVTOL CRP using the three-dimensional steady Reynolds-averaged Navier-Stokes solver and moving reference frames technique.

## 2. Proposed configuration

For urban on-demand air mobility, electric power sources are more advantageous than gas-powered propulsion. According to Moore and Fredericks, electric motors have a higher thrust-to-weight ratio than gas-powered jet engines due to having fewer heavy components. Electric engines are also much easier to scale up or down due to their relative simplicity[14]. This opens a number of possibilities to overcome aerodynamic and structural challenges posed by traditional aircraft. The downside of an octocopter is that they have a much larger planform area, and their efficiency can be reduced due to interaction between adjacent propellers[5]. An alternative approach is contra-rotating propellers.

In this study, the aircraft configuration is designed as follows:

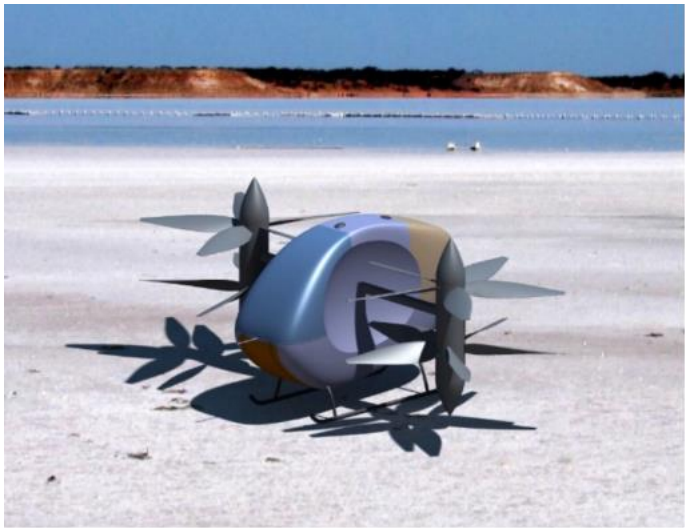

Figure 1 – Proposed configuration rendering

The parameters of the aircraft are shown in the table below:

Table 1 Parameters of the aircraft

| Parameters | Value |
|---|---|
| Aircraft length | 5m |
| Aircraft width | 2.5m |
| Aircraft height | 1.9m |
| Power unit diameter | 2m |
| Total weight | 1000kg |

The proposed configuration has the following characteristics:

1. The aircraft has compact shape and small floor area suitable for complex environment;

2. The fuselage is narrow in the middle and wide on front and rear side to reduce the shielding effect on the propeller;

3. To improve the utilization rate of the structure, the tilting shaft is shared by the power units on both sides;

## 3. Single and Dual Propellers power characteristics

In this chapter, the propeller momentum theory and CFD actuator disc method are used to calculate the ideal thrust of single propeller and dual propellers in different power consumptions.

The propeller momentum theory is based on the change in momentum and energy of the airflow passing through the propeller which is regarded as a disc with an infinite number of advancing propeller blades. The airflow continuously passes through the propeller disc. The thrust distribution on the propeller disc is uniform. Axial velocities before and after the disc are equal (regardless of the thickness of the paddle), in addition, there is no torque on the disc, and no rotation of the airflow through the disc[5]. For the convenience of solving, the gas is assumed to be an ideal incompressible fluid. In the momentum theory, the flow of airflow through the disc is shown in Fig. 3.

Although the propeller momentum theory reveals the thrust characteristics of single propeller and dual propellers in ideal conditions, the interference between upper and lower propeller is imprecise. In order to consider the interference between two propellers, the CFD actuator disc method is adopted.

The actuator disc method (ADM) is a widely used design and analysis tool, which plays an important role in predicting flow fields, propeller efficiency and simulating wind tunnel experiments. Georg Raimund Pirrung et al. used the ADM to simulate wind turbines with corrections for tip losses[16]; R. Bontempo and M. Manna performed a detailed numerical evaluation of the actuator disc method for split propellers[17]; Gijs AM van Kuik compares the flow of a actuator disc simulating a wind turbine and a propeller. Pierre-Elouan Réthoré et al. presents a general flexible method to redistribute wind turbine blade forces as permeable body forces in a computational domain，The special case of the actuator disc is successfully validated with an analytical solution for heavily loaded turbines and with a full-rotor computation in computational fluid dynamics[18].

### 3.1 Propeller momentum theory

In the propeller momentum theory, the flow of airflow through the disc is shown in Figure 2.

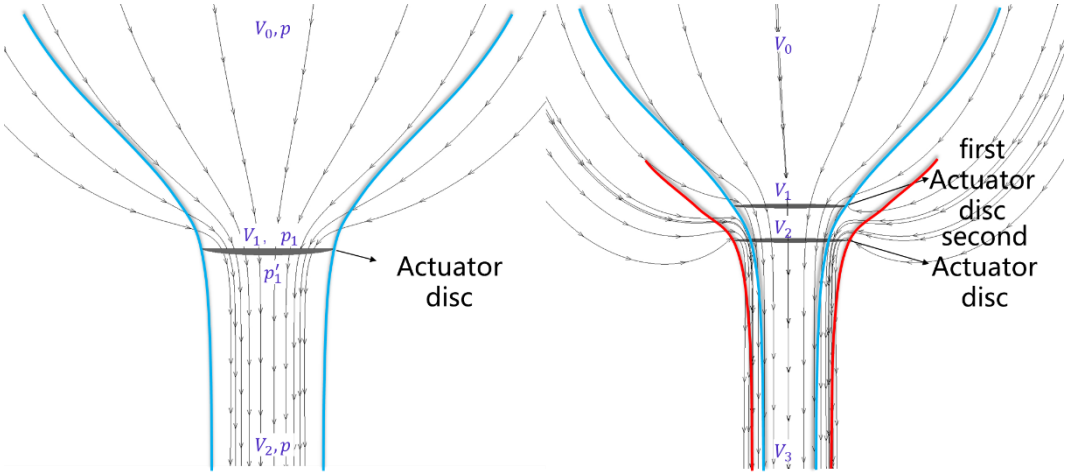


Figure 2- Flow model of single and dual discs

According to Bernoulli's equation, the following equation can be obtained:

$$P_0 + \frac{1}{2}\rho V_0^2 = P_1 + \frac{1}{2}\rho V_1^2 \tag{1}$$

$$P_1 + \frac{1}{2}\rho V_1^2 = P_2 + \frac{1}{2}\rho V_2^2 \tag{2}$$

$$P_2 + \frac{1}{2}\rho V_2^2 = P_3 + \frac{1}{2}\rho V_3^2 \tag{3}$$

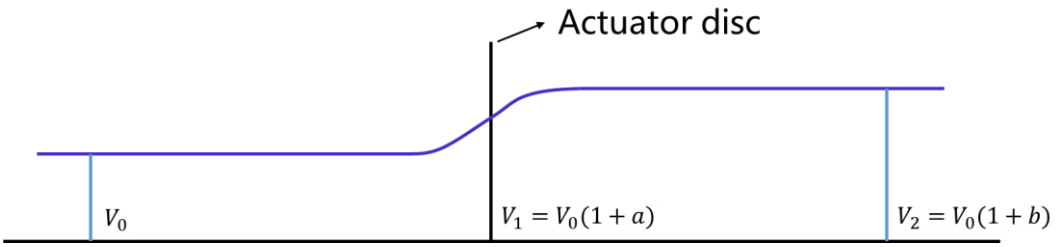


Figure 3- Velocity development diagram

For a single actuator disc, the velocity expression before the actuator disc is as follows:

$$V_1 = (1+a)V_0 \tag{4}$$

$$p + \frac{1}{2}\rho V_0^2 = p_1 + \frac{1}{2}\rho V_1^2 = p_1 + \frac{1}{2}\rho V_0^2(1+a)^2 \tag{5}$$

The expression for the velocity behind the actuator disc is as follows:

$$V_2 = (1+b)V_0 \tag{6}$$

$$p_1 + \Delta p + \frac{1}{2}\rho V_0^2(1+a)^2 = p + \frac{1}{2}\rho V_2^2 = p + \frac{1}{2}\rho V_0^2(1+b)^2 \tag{7}$$

The pressure difference before and after the actuator disc is as follows:

$$\Delta p = p_1' - p_1 = \left[p + \frac{1}{2}\rho V_0^2(1+b)^2\right] - \left[p + \frac{1}{2}\rho V_0^2\right] = \rho V_0^2 b\left(1 + \frac{b}{2}\right) \tag{8}$$

Assuming that the area of the actuator disc is A, the thrust generated by the actuator disc can be written in the following form:

$$T = A\Delta p = A\rho V_0^2 b\left(1 + \frac{b}{2}\right) \tag{9}$$

In addition, it can be known from the momentum theorem that the force of the actuator disc on the airflow (equal in magnitude and opposite to the thrust T of the actuator disc) should be equal to the increment of momentum passing through the actuator disc per unit time.

$$T = \rho A V_0(1+a)[V_0(1+b) - V_0] = \rho A V_0^2(1+a)b \tag{10}$$

$$A\rho V_0^2 b\left(1 + \frac{b}{2}\right) = A\rho V_0^2 b(1+a) \tag{11}$$

$$a = \frac{1}{2}b \tag{12}$$

From the above derivation, it can be concluded that the velocity increment at the actuator disc is half of the slip velocity increment.

Ideal efficiency refers to the ratio of the useful work done by the propeller thrust per unit time to the total amount of work done by the propeller to the airflow. The total work done by the propeller to the airflow per unit time can be represented by the kinetic energy increment of the airflow through the actuator disc.

$$\Delta E = \frac{1}{2}\rho A V_0(1+a)[V_0^2(1+b)^2 - V_0^2] = \rho A V_0^2 b(1+a)^2 \tag{13}$$

The useful work done by the propeller is as follows

$$\Delta E_1 = TV_0 = \rho A V_0^3 b(1+a) \tag{14}$$

$$\eta = \frac{TV_0}{\Delta E} = \frac{\Delta E_1}{\Delta E} = \frac{1}{1+a} \tag{15}$$

Ideally, the thrust expression obtained by the momentum theorem is as follows：

$$T = \rho A V_0^2 (1+a) b = 2\rho A V_0^2 (1+a) a \tag{16}$$

Substituting the above formula into the efficiency expression, the following expression can be obtained:

$$T = \frac{2\rho A V_0^2 (1-\eta)}{\eta^2} \tag{17}$$

$$C_T = \frac{T}{\frac{1}{2}\rho V_0^2 A} = \frac{T}{qA} \tag{18}$$

The ideal efficiency in the forward flight state as follows：

$$\eta = \frac{2}{C_T}\left(\sqrt{1+C_T} - 1\right) \tag{19}$$

The hover efficiency defines as follows:

$$\eta_{hover} = \sqrt{\frac{2}{\pi}} \frac{C_T}{C_P} \tag{20}$$

For the hovering state, the formula for calculating the ideal hovering power can be obtained as follows：

$$P_{hoverideal} = T\sqrt{\frac{T}{2\rho A}} \tag{21}$$

The second actuator disc is in the wake of the first actuator disc, the second actuator disc is in a forward flying state. The wake velocity can be calculated from the primary momentum disc as the incoming velocity of the secondary actuator disc.

$$V_{induced} = \sqrt{\frac{T}{2\rho A}} \tag{22}$$

$$V_2 = V_{induced} \times K \tag{23}$$

$$K = \frac{D}{D - 0.3 \times \Delta H} \tag{24}$$

Through the above analysis and calculation, we can obtain the power characteristics of single and dual propellers under ideal conditions as follows:

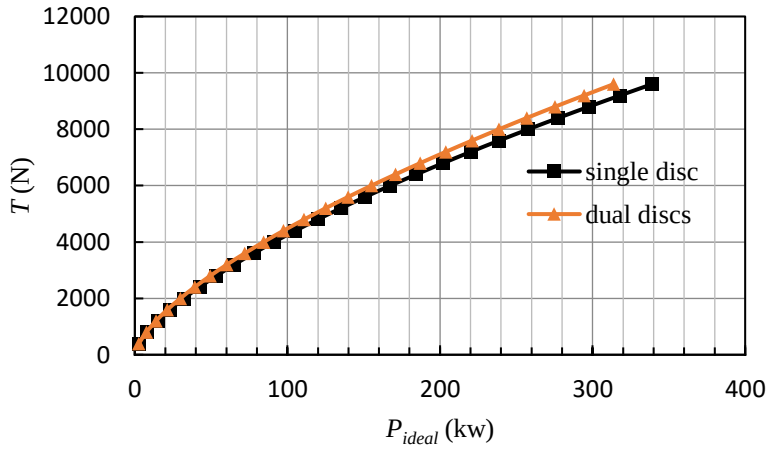


Figure 4 - Ideal thrust of single and dual discs (propeller momentum theory)

As can be seen from the above figure, dual actuator discs can generate more thrust than the single actuator disc consuming the same power. As the power gradually increases, the high thrust advantage of the dual actuator discs becomes obvious. However, the momentum theory does not consider friction, and only empirical formula can be used to estimate the axial velocity between two actuator discs. In order to improve the calculation accuracy, CFD actuator disc method is used to simulate the real actuator disc flow field.

## 3.2 CFD actuator disc method

In this section, the CFD actuator disc method is used to simulate the ideal propeller flow field and obtain more precise efficiency to verify the results of the momentum method.

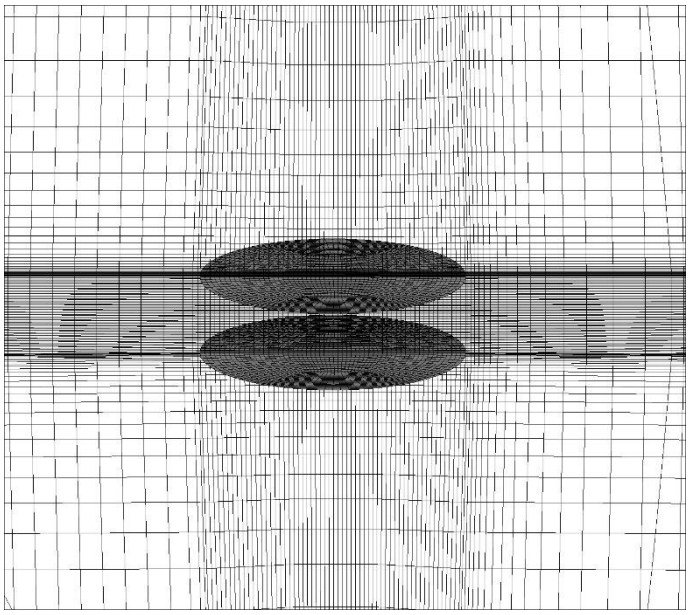

Figure 5 - CFD actuator disc model

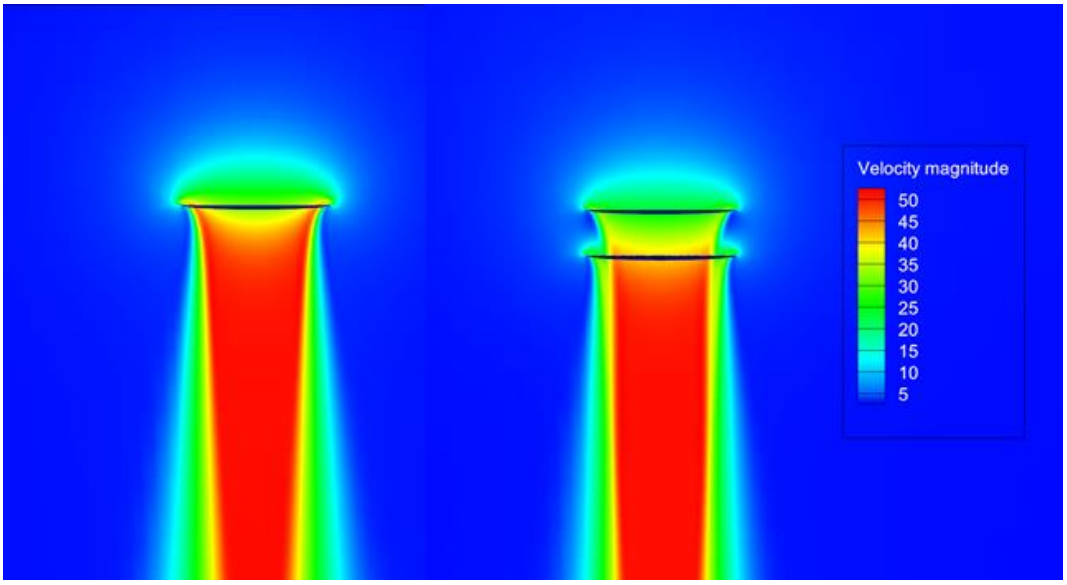


Figure 6 - CFD actuator disc velocity magnitude contours

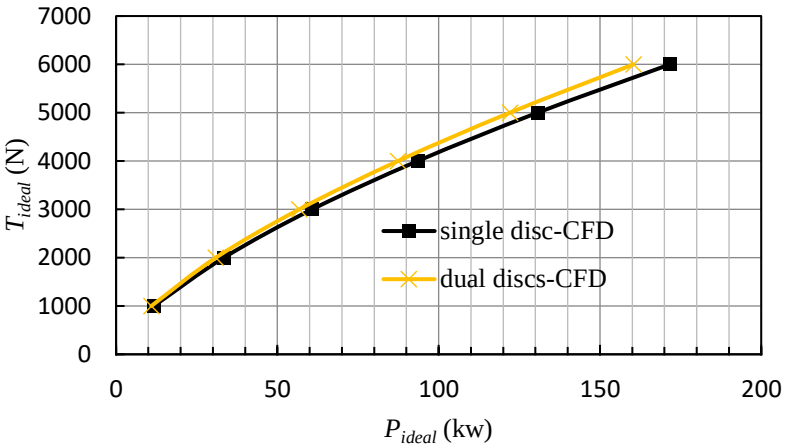


Figure 7 - Ideal thrust of single and dual discs (CFD actuator disc method)

The error between the momentum theory calculation results and actuator disc CFD simulation results is within 3%.

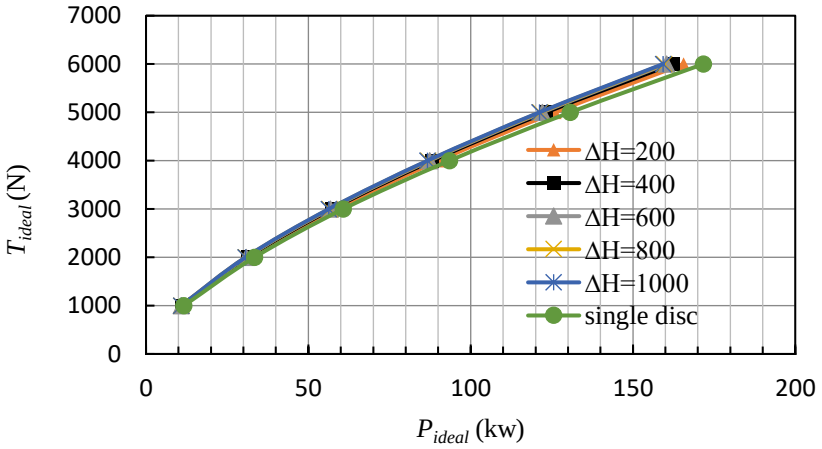


Figure 8 - Ideal thrust of single and dual discs with different spacing

The figure above shows the residual power of different axial distances compared with the single disc with the same thrust. The residual power of dual disc increases with the disc spacing. However, when the disc axial distance exceeds 600mm ($\Delta h/D > 0.3$), the residual power growth rate gradually decrease.

## 4. Propeller design optimization

This chapter focuses on the design and optimization of propellers for the given aircraft configuration. For the single propeller, the hover state is used as the design input. For the CRPs, the design is based on the equal thrust distribution, the upper propeller is the same as the single propeller.

In the design and optimization process, the BEM method and the CFD method were selected as the rough model and the fine model for the propeller aerodynamic calculation. The surrogate model is constructed by the rough model, and the pointer optimization method is used for optimization.

### 4.1 Blade Element momentum method

The BEM method integrates the blade element theory and momentum theory. In the momentum theory, the propeller is simplified as a disc without thickness, and the thrust and power of the propeller are obtained by the conservation of momentum. In the blade element theory, the blade unit is divided into several micro-segments along the span, and the aerodynamic force of each micro-segment is replaced by the airfoil aerodynamic force, in addition, the thrust and torque of each micro-segment can be obtained by calculating the airfoil aerodynamic force.

$$dT = \frac{1}{2} B\rho V^2 (C_L cos\varphi - C_D sin\varphi) cdr \tag{25}$$

$$dQ = \frac{1}{2} B\rho V^2 (C_L sin\varphi - C_D cos\varphi) crdr \tag{26}$$

However, in reality, this flow is strongly 3D, which results in a pronounced flow around the tip. In addition, this method also neglects the interference effects between successive blade elements. These assumptions result in errors in propeller thrust and torque calculations and consequently in performance prediction.

In order to simulate a real propeller with a finite number of blades, tip loss effects are introduced into the BEM method by using the Prandtl tip loss.

$$F = \frac{2}{\pi} COS^{-1} \left[ exp\left( -\frac{B(R-r)\sqrt{1+\lambda^2}}{2R} \right) \right] \tag{27}$$

Where $\lambda = \Omega R / U_\infty$ is the tip speed ratio.

## 4.2 Optimization Parameters

The input parameters to this model are as follows: the distributions of the chord length (c) and pitch angle ($\beta$) along the blade radius, the propeller rotational speed (rpm), the thrust required, the distribution of the axial velocity (for lower propeller) and the particular cross-sectional airfoil. Given these inputs, the program goes through an iterative process to determine the induced velocities which are then used to determine the relative inflow angle $\varphi$, hence the local angle of attack $\alpha$. The thrust and torque coefficients, $C_T$ and $C_q$, are then obtained using the airfoil characteristics.

Usama T Toman et al. stated that only three sections are sufficient for the design optimization[19]. Since this study is mainly aimed at optimizing the contra-rotating propeller, the inflow conditions of the secondary rotor are relatively complex, so four sections are used for design and optimization.

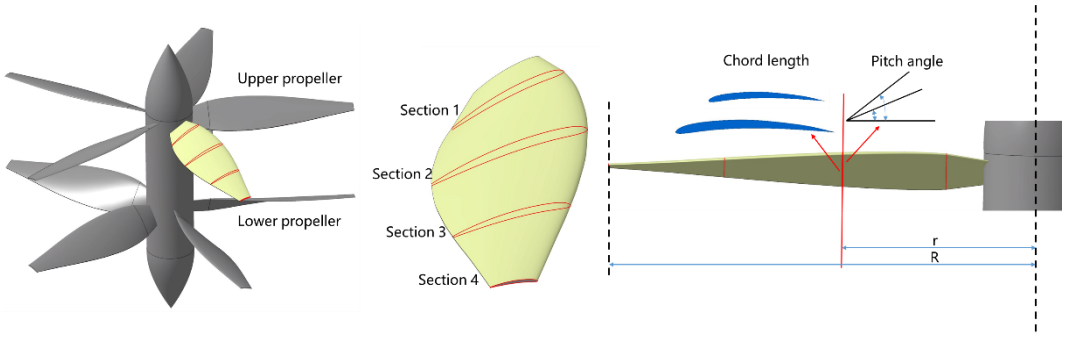


Figure 9 - Design parameters

## 4.3 Design Optimization Algorithm

In this paper, A CRP design optimization method is proposed with the actuator disc method and the BEM. Once the proposed configuration is determined, we develop appropriate propeller design inputs and airfoil based on the requirements of the aircraft. The aerodynamics of the airfoil at different Reynolds numbers and Mach numbers is calculated by CFD method. For the single propeller and upper propeller in CRP, we use Design of Experiments (DOE) techniques to determine the sample points calculated by the BEM method.

The Radial Basis Function (RBF) is used to generate the response surface. RBF approximation is a type of neural network employing a hidden layer of radial units and an output layer of linear units. RBF approximations are characterized by reasonably fast training and reasonably compact networks. They are useful in approximating a wide range of nonlinear spaces[20]. The optimization was carried out with Pointer Automatic Optimizer and the optimized blade shape is generated.

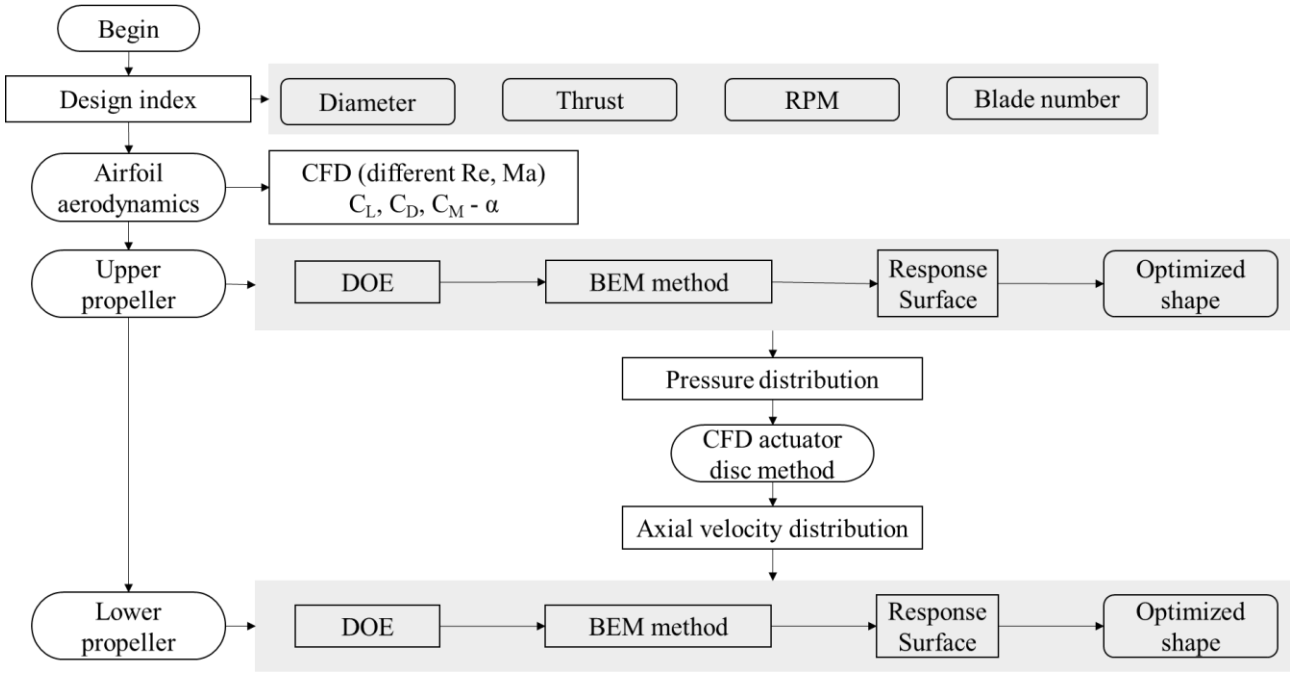


Figure 10 – Optimization algorithm

## 4.4 Single Propeller Design Process

In order to satisfy the flight requirements of the aircraft, the design input of the single propeller is proposed as follows:

Table 1 Design index

| Single propeller | |
|---|---|
| Parameter | Design index |
| max thrust | 5500N |
| diameter | 2m |
| airfoil | ARAD-006 |
| rpm | 1600 |

The Latin hypercube is used to extract sample points from the range of variable values, and the BEM method is used to calculate the response surface.

The value ranges of optimization variables are shown in the following table:

Table 2 Single propeller design scope

| Single propeller | | |
|---|---|---|
| r/R | Chord length/m | Pitch angle |
| 0.235 | 0.15 ~ 0.25 | 22° ~ 35° |
| 0.5 | 0.2 ~ 0.35 | 15° ~ 25° |
| 0.8 | 0.15 ~ 0.25 | 10° ~ 20° |
| 1 | 0.05 ~ 0.15 | 3° ~ 10° |

The optimization results of the single propeller are shown in the following table:

Table 3 Single propeller optimization result

| Single propeller | | |
|---|---|---|
| r/R | Chord length/m | Pitch angle |
| 0.235 | 0.2 | 26.85° |

| | | |
|---|---|---|
| 0.5 | 0.26 | 18.9° |
| 0.8 | 0.184 | 12.9° |
| 1 | 0.075 | 4.58° |

## 4.5 Contra-rotating Propeller Design

The design of the contra-rotating propeller focuses on the design optimization of the lower propeller, the upper propeller directly adopts the design result of the single propeller.

The incoming flow condition of the lower propeller is different from that of the single propeller. Due to the existence of the upper propeller, the lower propeller is under the incoming flow of a certain axial velocity distribution. The accuracy of the axial velocity distribution directly affects the design of the secondary propeller. In this study, the CFD actuator disc method is used to extract the axial velocity distribution of a specific section as the input of the incoming velocity of the lower propeller.

In Chapter 2, the CFD actuator disc method is used to compare the efficiency differences of different thrust and disc spacing. In this section, the same method will be used to obtain the axial velocity distribution. Designed for hovering state points, the upper and lower propeller provide the same thrust equal to 2500N.

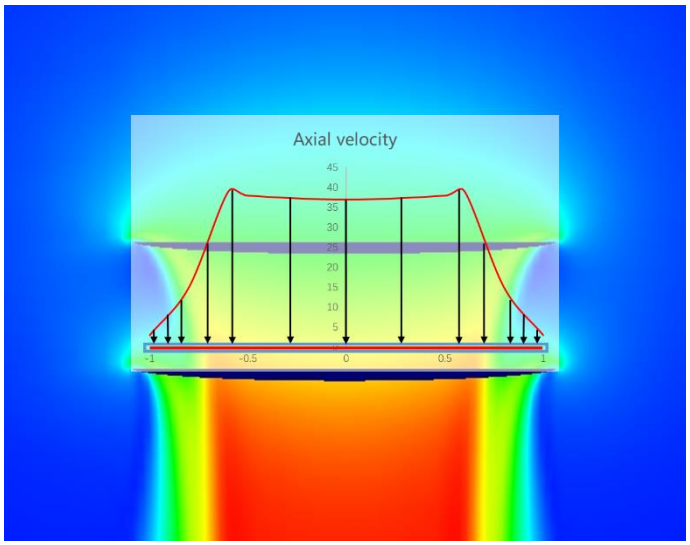


Figure 11 - Axial velocity distribution

After calculating the incoming flow velocity, the design and optimization of the lower propeller is carried out by using a similar method for the single propeller. First, the variable range of the lower propeller blade is determined according to the incoming flow speed as follows:

Table 4 Lower propeller design index

| Lower propeller | |
|---|---|
| r/R | Pitch angle |
| 0.235 | 40° ~ 55° |
| 0.5 | 30° ~ 40° |
| 0.8 | 20° ~ 30° |
| 1 | 5° ~ 15° |

The Latin hypercube is used to extract sample points from the range of variable values, and the BEM method is used to calculate the response surface. The optimal solution is obtained by the pointer optimization method. The final optimization results are shown in the following table:

Table 5 Lower propeller optimization result

| Lower propeller | |
|---|---|
| r/R | Pitch angle |
| 0.235 | 50° |
| 0.5 | 34.38° |
| 0.8 | 25.95° |
| 1 | 10° |

## 5. Results and Discussion

To validate the present method, CFD results of the single propeller, ordinary contra-rotating propeller (the upper and lower propeller are the same) and optimized contra-rotating propeller are analyzed in this chapter, in addition, a detailed parametric study is conduced to illustrate how the rpm influence the efficiency of the contra-rotating propeller.

### 5.1 Contra-rotating Propeller Design

In this study, CFD simulation is used as a high-fidelity detailed model to accurately predict the performance of the propeller. The steady RANS solver is used to conduct the CFD simulations. The Shear Stress Transport (SST) model is used for the closure of the Reynolds stresses. The Multiple Reference Frame (MRF) is adopted as the effective method for steady calculation of fluid rotational motion. The MRF method divide the grid of the static area and the rotating area into two parts, and simplify the flow field in the rotating area where the propeller is located as the instantaneous flow field of the blade at a certain moment to solve and the static area still uses the inertial frame as the reference frame, and a local reference frame is used at the interface of the two areas to transfer the flux on the calculated boundary of one adjacent area to the boundary of another area, so that the unsteady problem is transformed into a steady problem for calculation.

The grid model adopts periodic grid, and two rotation domains with opposite rotation directions are set inside.

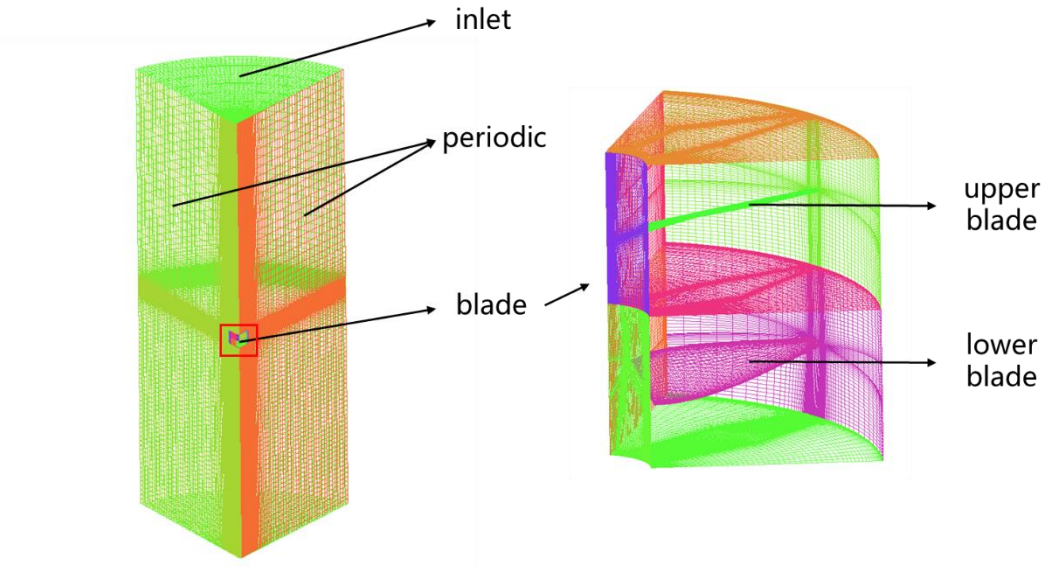


Figure 12 - Propeller CFD model

### 5.2 CFD method validation

In order to verify the accuracy of the MRF model for simulating the rotor flow field, an existing propeller[21] was selected to conduct a 1:1 model experiment. The test bench is shown in Figure 13 MRF method is used to compare with the experiment. From Figure 14, it can be seen that the thrust

and torque data calculated by the MRF model is slightly larger than the experimental data, but the error is always within 5%, which proves that the results of the MRF model have high reliability.

Figure 13 - Propeller test bench

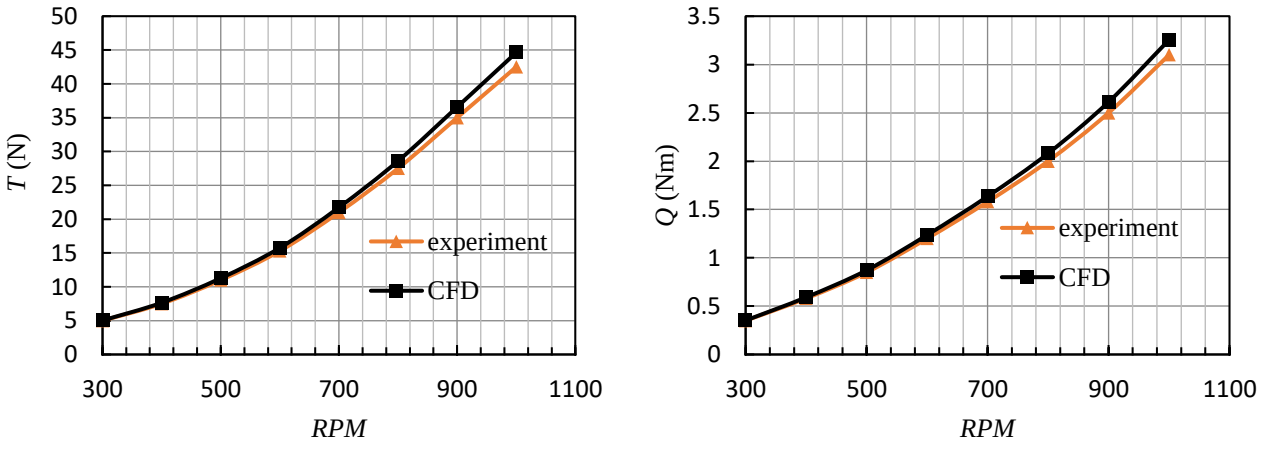


(a) Propeller thrust (b) Propeller torque

Figure 14 - Thrust and torque of experiment and CFD

## 5.3 Results and Discussions

In this section, the single propeller, ordinary contra-rotating propeller and optimized contra-rotating propeller are calculated by the aforementioned method. In addition, a detailed parametric study is conduced to illustrate how the rpm influence the efficiency of the contra-rotating propeller.

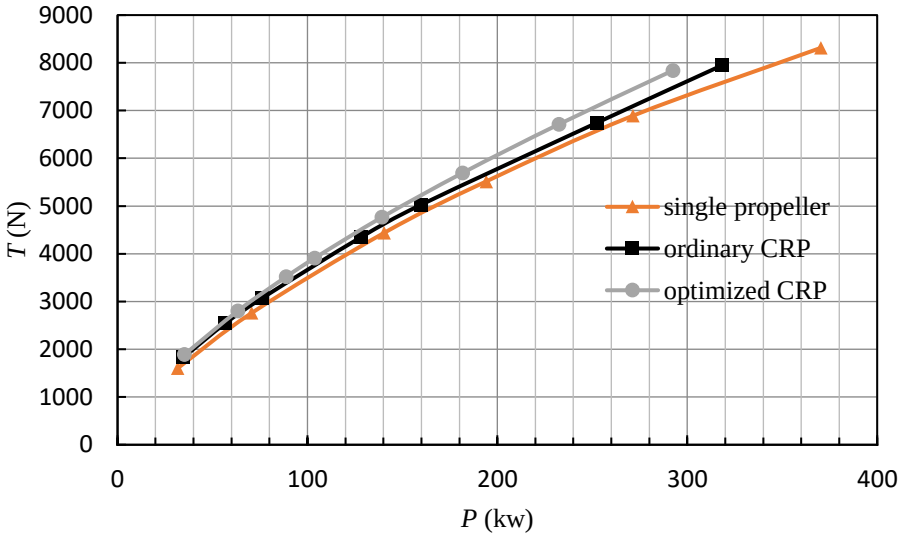


Figure 15 - Thrust of single propeller, ordinary CRP and optimized CRP

## 5.4 Hovering time benefit

The optimized contra-rotating propeller increases the efficiency of the propulsion system, but also increases the structural weight ratio. The weight distribution of the aircraft is analyzed to determine the endurance benefits from the increased efficiency of the propulsion system.

The weight difference between the CRPs and single propeller is mainly generated by the weight difference of the motor and the propeller.

The specific power of the electric motor is 4. The maximum power of the motor is 200kw in a single-propeller aircraft, and 85kw in the CRP aircraft.

Table 6 Weight Comparison (Single propeller aircraft and CRP aircraft)

| | | Single propeller | | Contra-rotating propeller | |
|---|---|---|---|---|---|
| Sub-system | Devices | Number | Weight (kg) | Number | Weight (kg) |
| Aircraft control system | Rudder | 2 | 5 | 4 | 10 |
| | 12S battery | 1 | 5 | 1 | 5 |
| | Wires and Cables | 1 | 30 | 1 | 30 |
| | Other equipment | | 5 | | 5 |
| Aircraft structure | Fuselage structure | 1 | 70 | 1 | 70 |
| | Tilting structure | 1 | 35 | 1 | 35 |
| | Landing gear | 1 | 20 | 1 | 20 |
| Propulsion system | MCU | 1 | 8.5 | 1 | 8.5 |
| | Propeller | 2 | 50 | 4 | 60 |
| | Motor | 2 | 100 | 4 | 85 |
| | Battery | 1 | 591.5 | | 591.5 |
| | Water Pump/Tank | 1 | 10 | 1 | 10 |
| Payload | | 1 | 70 | 1 | 70 |
| Total weight | | | 1000 | | 1000 |

After weight distribution and calculation, the battery weight of both configurations is 591.5kg and the total capacity is 118300wh (200Wh/kg). In the hovering state, the propulsion system needs to provide 11,000N thrust with the single propeller power of 388 kW and the CRP power of 344 kW. The hovering time is 30 minutes for the single propeller aircraft and 34 minutes for the CRP aircraft. The hovering time of the CRP aircraft is 12.7% higher than the hovering time of the single propeller aircraft.

## 6. Conclusions

The hovering power of the eVTOL UAV has a significantly important impact on the endurance time. Efficient propellers can significantly improve the endurance of the UAV. The ideal efficiency of the dual propellers and single propeller are calculated using the momentum theory and CFD actuator disc method, which verify the efficiency potential of the dual propellers. A CRP is designed based on the proposed UAV configuration which is verified by validation cases on an eVTOL CRP using the three-dimensional steady Reynolds-averaged Navier-Stokes solver and moving reference frames technique. The CFD results show that the optimized CRP hovering time is 12% higher than that of the single propeller.

Some main conclusions include:

1) It is practical to use the actuator disc to simulate the flow of the upper and lower propellers especially the axial velocity distribution.
2) The axial velocity distribution obtained by the CFD actuator disc method can be used as the velocity input of the lower propeller.
3) The optimized CRP hovering time is 12% higher than that of the single propeller.

## 7. Contact Author Email Address

Nanxuan Qiao: qiaonanxuan@buaa.edu.cn

## 8. Copyright Statement

## References


[1] Piccinini R, Tugnoli M and Zanotti A. Numerical Investigation of the Rotor-Rotor Aerodynamic Interaction for eVTOL Aircraft Configurations. *Energies (Basel).* Vol. 13, No. 1, pp 59-95, 2020.

[2] Sahoo S, Zhao X and Kyprianidis K. A Review of Concepts, Benefits, and Challenges for Future Electrical Pro-pulsion-Based Aircraft. *Aerospace*. Vol. 7, pp 44, 2020.

[3] Naldi R, Gentili L and Marconi L et al. Design and experimental validation of a nonlinear control law for a ducted-fan miniature aerial vehicle. *Control Engineering Practice.* Vol. 18, pp 747-760, 2010.

[4] Littell J D. Challenges in Vehicle Safety and Occupant Protection for Autonomous electric Vertical Take-off and Landing (eVTOL) Vehicles. *AIAA Propulsion and Energy Forum*, Indianapolis, No. 1, pp 1-16. 2019.

[5] Tinney C E, Sirohi J. Multirotor Drone Noise at Static Thrust. *AIAA Journal*. Vol. 56, No. 7, pp 2816-2826, 2018.

[6] Mckay R S, Kingan M J, Go S T, et al. Experimental and analytical investigation of contra-rotating multi-rotor UAV propeller noise. *ACOUSTICS 2019*, Cape Schanck, Victoria, Australia, Vol. 177, No. 1, 2019.

[7] Yang X, Liu T and Ge S, et al. Challenges and key requirements of batteries for electric vertical takeoff and land-ing aircraft. *Joule*. Vol. 5, No. 7, pp 1644-1659, 2021.

[8] Polaczyk N, Trombino E and Wei, P. et al. A review of current technology and research in urban on-demand air mobility applications. *8th Biennial Autonomous VTOL Technical Meeting and 6th Annual Electric VTOL Symposium 2019,* pp. 333-343, 2019.

[9] Su S, Wang S, Cao J, et al. Prediction of hydrodynamic characteristics of combined propellers based on CFD method. *3rd International Conference on Fluid Mechanics and Industrial Applications*, Vol. 1300, No. 1, 2019.

[10] Toru, Junichiro and Hiroki. Influence of Blade Row Distance on Performance and Flow Condition of Contra-Rotating Small-Sized Axial Fan. *International Journal of Fluid Machinery and Systems*, Vol. 5, No. 4, 2012.

[11] Jung H, Kanemoto T, Liu P, et al. A numerical study on performance improvement of counter-rotating type tidal stream power unit. *29th IAHR Symposium on Hydraulic Machinery and Systems*, Vol. 240, No. 5, 2019.

[12] Tang J, Wang X, Duan D, et al. Optimisation and analysis of efficiency for contra-rotating propellers for high-altitude airships. *The Aeronautical Journal*, Vol. 123 No. 1263, pp 706-726, 2019.

[13] Lee S and Dassonville M, Iterative Blade Element Momentum Theory for Predicting Coaxial Rotor Performance in Hover, *Journal of The American Helicopter Society*, Vol. 65, pp 1-12, 2020.

[14] Moore M D and Fredericks B, Misconceptions of Electric Propulsion Aircraft and their Emergent Aviation Markets, *52nd Aerospace Sciences Meeting*, National Harbor, Maryland, 2014.

[15] Liu Peiqing, *Propeller theory and its applications*, 1st edition, Beihang University Press, 2006.

[16] Pirrung G R, Laan M P, Ramos García N, et al. A simple improvement of a tip loss model for actuator disc simulations, *Wind Energy*, Vol. 23, No. 4, pp 1154-1163, 2020.

[17] Bontempo R, Manna M. Actuator disc methods for open propellers: assessments of numerical methods, *Engineering applications of computational fluid mechanics*, Vol. 11, No. 1 pp 42-53, 2017.

[18] Réthoré P, van der Laan P, Troldborg N, et al. Verification and validation of an actuator disc model. *Wind Energy*, Vol. 17, Num. 6 pp 919-937, 2014.

[19] Toman U T, Hassan A S, Owis F M, et al. Blade shape optimization of an aircraft propeller using space map-ping surrogates, *Advances in Mechanical Engineering*, Vol. 11, No.7, 2019.

[20] Zhou L, Yan G, Ou J. Response Surface Method Based on Radial Basis Functions for Modeling Large-Scale Structures in Model Updating. *Computer-Aided Civil and Infrastructure Engineering*, Vol. 28, No. 3, pp 210-226, 2013.

[21] Ma Tl, Zhang Zl, Liu Zc et al. Tilt-rotor aircraft cruise state rotor slipstream effects . *Journal of Beijing*

*University of Aeronautics and Astronautics,* Vol. 47, No. 6, pp 1124-1137, 2021.